Letter

Spectrum analysis with parametrically modulated transmon qubits

Nir Gavrielov [1,*] Santiago Oviedo-Casado [2,3,†] and Alex Retzker [1,4,‡]
[1]Racah Institute of Physics, Hebrew University of Jerusalem, 91904 Jerusalem, Israel
[2]Área de Física Aplicada, Universidad Politécnica de Cartagena, E-30202 Cartagena, Spain
[3]Escuela Superior de Ingeniería y Tecnología, Universidad Internacional de La Rioja, 26006 Logroño, La Rioja, Spain
[4]AWS Center for Quantum Computing, Pasadena, California 91125, USA

(Received 15 July 2024; accepted 28 January 2025; published 6 March 2025)

Exploring the noise spectrum impacting a qubit and extending its coherence duration are fundamental components of quantum technologies. In this study, we introduce parametric spectroscopy, a method that merges parametric modulation of a qubit's energy gap with dynamical decoupling sequences. The parametric modulation provides high sensitivity to extensive regions of the noise spectrum, while dynamical decoupling reduces the effect of driving noise. Our theoretical study shows that parametric spectroscopy enables access to the difficult high-frequency domain of the flux spectrum in transmons.

DOI: 10.1103/PhysRevResearch.7.L012056

Introduction. Preserving quantum states long enough to realize quantum operations is a challenging task. Noise, which causes internal system relaxation and the reduction of coherence, is one of the major hurdles that aspiring quantum technologies face [1], and has sparkled a myriad of noise mitigation techniques based on sophisticated forms of dynamical decoupling (DD) [2–9]. The basic working principle of DD is to create customized frequency filters that reduce the harmful impact of uncontrolled degrees of freedom [10–12], resulting in longer coherence times. Owing to this frequency selectivity, the same protocols can, in principle, be used for noise spectroscopy [13–16].

Superconducting qubits (SQs) are one of the main platforms to enact quantum technologies, in which high-fidelity gate operations and long coherence times are routinely achieved. A precise and detailed knowledge of the noise spectrum and its impact on the system is crucial, and for that reason a whole body of work has tried to unveil the different noise sources affecting superconducting qubits [14,17–21]. However, transmons find it difficult to access the high-frequency region of the noise power spectrum and can generally only achieve frequencies up to a few hundred MHz, thereby leaving large portions of the spectrum inadequately explored. It is possible to reach the high-frequency range by tuning the energy gap [14,22]; however, such a technique suffers from low signal-to-noise ratio (SNR). Another option is to utilize spin locking on the flux qubit, which has significant nonlinearity, to attain Rabi frequencies in the GHz range [18,23].

Interestingly, relaxometry analysis of the high-frequency noise spectrum displays an Ohmic behavior around the SQ natural energy gap of 5–6 GHz [24], in stark contrast with the $1/f$ spectrum observed at low frequencies [25]. Methods for reliably accessing the unknown regions of the SQ noise spectrum are imperatively needed.

Among SQ families, the tunable transmon features a flexible energy gap that can be parametrically modulated to resonate with another SQ using an oscillating radio-frequency flux [26–28], thereby favoring gate creation with great flexibility and state-of-the-art fidelity [26,28–35]. The transmon possesses static and dynamical sweet spots, specific energy gaps at which the transmon becomes relatively insensitive to flux noise, attaining long coherence times [17,36]. Here, we aim to utilize the fact that during frequency modulation around the static sweet spots, tunable transmons behave as frequency filters, potentially serving as accurate noise spectrometers while maintaining long coherence.

In this Letter, we suggest integrating microwave pulsed dynamical decoupling sequences within parametric modulation, enabling spectrum sampling at any desired modulation frequency. This approach facilitates high-resolution noise spectroscopy across a broad spectral range, from a few MHz to GHz. We begin by introducing the fundamental concept of *parametric spectroscopy*, demonstrating its operating principle in a tunable transmon. Subsequently, we theoretically and numerically exhibit unmatched spectral resolution at the high-frequency end of the spectrum, a region that has previously resisted most probing efforts. Moreover, we show a substantial improvement in coherence time along with minimized leakage to higher-energy levels. The versatility of the protocols we investigate implies that parametric spectroscopy can be utilized with any qubit possessing a tunable energy gap. This opens opportunities for noise spectroscopy across various setups and provides a tool for achieving

*Contact author: nir.gavrielov@mail.huji.ac.il
†Contact author: oviedo.cs@mail.huji.ac.il
‡Contact author: retzker@phys.huji.ac.il

Published by the American Physical Society under the terms of the Creative Commons Attribution 4.0 International license. Further distribution of this work must maintain attribution to the author(s) and the published article's title, journal citation, and DOI.

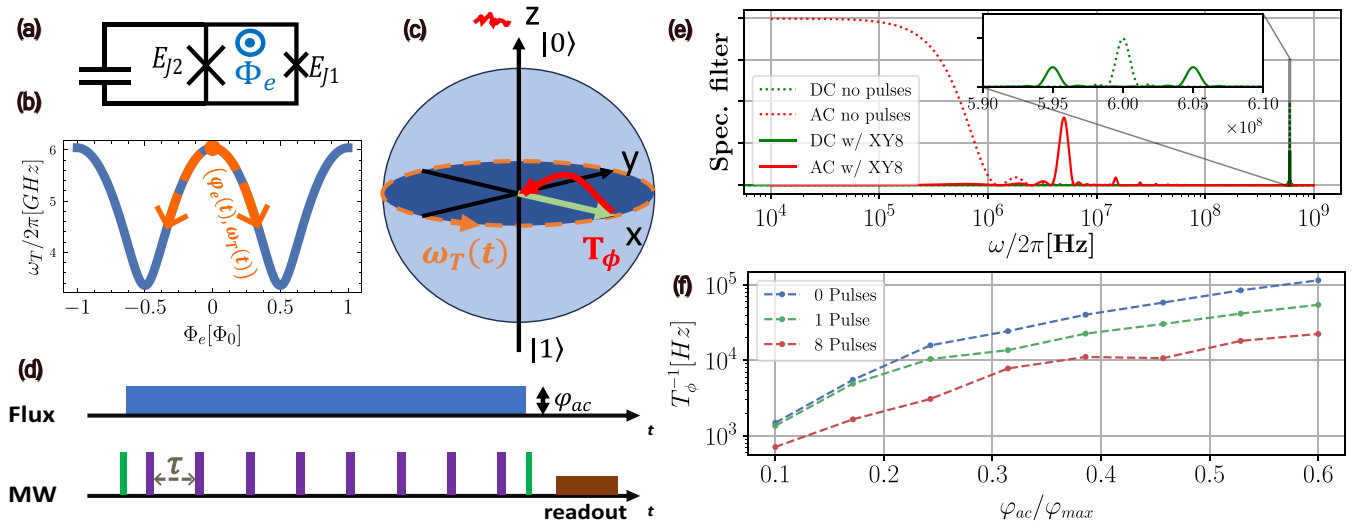


FIG. 1. (a) Schematic tunable transmon circuit. (b) Qubit energy curve, with an illustration of parametric modulation (orange) of the transmon energy gap. (c) Bloch sphere depiction of dephasing during parametric modulation. The Bloch vector (green) of a superposition state rotates around the polarization axis at an angular frequency that matches the energy gap ω_T. Longitudinally coupled noise (red) causes loss of phase information. Tuning of the energy gap through ω_m permits matching ω_T to specific noise frequencies that are detected. (d) Sketch of a parametric spectroscopy sequence with a pulse train on both the flux and the microwave channels. (e) Spectral filters for the additive (DC, green) and multiplicative (AC, red) noise sources during parametric spectroscopy. Solid lines show the filters when an additional *XY*8 sequence is applied, shifted from the original parametric modulation spectrum (dashed). (f) Dephasing rate T_ϕ^{-1} of the modulated qubit ($\frac{\omega_m}{2\pi} \approx 500$ MHz) from numerical simulations, where $\varphi_{\max} = \pi/2$ marks the first minimum of $\omega_T(\varphi_e)$. Adding concurrent dynamical decoupling pulses filters out unwanted noisy frequencies, with the immediate consequence of decreasing the dephasing rate, as shown by the application of a single π rotation (Hahn echo), as compared to parametric modulation without DD pulses (dashed blue). Applying an *XY*8 DD sequence provides up to a fivefold decrease in the dephasing rate in a point-by-point comparison with bare parametric modulation. Such a decrease amounts to a fivefold increase in coherence time when compared to state-of-the-art parametrically modulated transmons [35,37].

extended coherence times, an essential resource for quantum technologies.

Parametric spectroscopy. We begin by describing the method operating in a transmon device, considered for now as a two-level system with an energy gap $E_{01} = \hbar\omega_T$. The qubit frequency ω_T is periodically controlled by an external flux Φ_e threading the superconducting quantum interference device (SQUID) loop shown in Fig. 1(a) [38]. Parametric modulation of the transmon stands for applying a sinusoidal drive,

$$\varphi_e(t) = \varphi_{dc} + \delta\varphi_{dc}(t) + [\varphi_{ac} + \delta\varphi_{ac}(t)]\sin(\omega_m t), \qquad (1)$$

of modulation frequency ω_m, through the flux channel, with $\varphi_e \equiv \pi\Phi_e/\Phi_0$, normalized to the flux quantum unit Φ_0. The qubit response around a sweet spot—shown in Fig. 1(b)—is, approximately, quadratic:

$$\omega_T(\varphi_e) \simeq \omega_T(0) + b_0\varphi_e^2, \quad b_0 \equiv \frac{1}{2}\frac{\partial^2\omega_T(\varphi_e)}{\partial\varphi_e^2}, \qquad (2)$$

in which b_0, the curvature around the peak, depends on the capacitive (E_C) and junction (E_{J1}, E_{J2}) energies of the circuit. The net result is that the qubit becomes maximally sensitive to additive environmental noise frequencies that match the modulated qubit energy gap, henceforth DC noise $\delta\varphi_{dc}$, while being desensitized to the rest of the environment spectrum. Thus, for typical transmon parameters, the sensitivity of parametric modulation to a pure tone signal is on par—$2\varphi_{ac}/3$—with that of an optimal spin-locking sequence (see Sec. II of the Supplemental Material (SM) [39]). On the other hand, it means that the qubit is additionally subjected to multiplicative AC noise $\delta\varphi_{ac}$ introduced by the flux modulation amplitude.

Interaction with noise causes qubit frequency fluctuations which, when the system is prepared in an initial superposition state, result in dephasing, whose characteristic time T_ϕ is defined through the decoherence function $W(t) \equiv |\langle\exp[-i\int_0^t \delta\omega_T(t')dt']\rangle|$ as $W(T_\phi) = 1/e$ [7]. Throughout this work, we assume Gaussian noise and ignore possible noise relaxation effects, focusing on the $T_1 \gg T_\phi$ regime [25]. The coupling of the noise terms to an oscillating signal leads to a frequency shift in the spectral domain, as shown in Fig. 1(e). As a result, the dephasing of the qubit depends on the spectrum of the environmental noise at the modulation frequency,

$$-\ln W(t) \simeq b_0^2\varphi_{ac}^2 t\left[S_{dc}(\omega_m) + \frac{1}{4}S_{ac}(2\omega_m)\right] + \frac{b_0^2\varphi_{ac}^2 t^2}{2}\int_{-\infty}^{\infty}\frac{d\omega}{2\pi}\mathrm{sinc}^2\left(\frac{\omega t}{2}\right)S_{ac}(\omega), \qquad (3)$$

with $S(\omega)$ the power spectral density at a frequency ω. A detailed derivation of the decoherence function can be found in Sec. I in the SM [39].

Experimental evidence suggests a strong decoherence contribution from electronic (multiplicative) noise [34], which typically has a $1/f$ spectrum with lower (upper) $\omega_{ir}(\omega_{uv})$ cutoff, which we assume from now on. Then, the zero-frequency multiplicative noise [the last term in Eq. (3)] overshadows the target signal $S_{dc}(\omega_m)$, as depicted in Fig. 1(e), causing

low SNR for frequency detection through parametric modulation, limiting its scope to low frequencies that require small modulation amplitudes. We overcome the difficulty by concurrently applying a microwave pulsed DD sequence that reduces the impact of the multiplicative process while keeping the sensitivity to the additive target signal intact. Considering a series of equidistant impulsive π rotations separated by a delay time τ, as sketched in Fig. 1(d), causes the additive and multiplicative spectral filters due to parametric modulation to split onto two windows, each shifted by $\pm\omega' = \pi/\tau$ from its original central frequency [see Fig. 1(e)] [7,14]. Typical DD sequences shift the frequency by a few MHz, pushing the multiplicative noise away from the origin, but only slightly affecting the parametric filter, which is at least tens of MHz. Consequently, the filter becomes increasingly precise, permitting larger modulation amplitudes that allow reaching the high-frequency spectrum and achieving, at the same time, a significant reduction of dephasing, as we demonstrate in Fig. 1(f) (see SM [39]). There, we consider both a Hahn echo (single π rotation) and the paradigmatic *XY*8 DD sequence, which minimizes possible pulse errors by alternating the π rotations around the different axes of the Bloch sphere, thereby partially compensating the error of a given pulse by the other pulses in the sequence [8]. The addition of this *XY*8 DD sequence to parametric modulation offers a fivefold increase in the dephasing time T_ϕ compared to bare parametric modulation, owing to the frequency selectivity introduced by the DD sequence, which significantly reduces the impact of the noisy environment. The extended dephasing time results in further improvement in the sensitivity,

$$S^p_{dc_{\min}}(\omega_m) \approx \frac{\mathrm{e}}{2Cb_0^2\varphi_{ac}^2\sqrt{T_\phi}}, \tag{4}$$

where C is the overall readout efficiency parameter. A better trade-off between the strength of the noise signal (through φ_{ac}) and the coherence time can be achieved to obtain state-of-the-art sensitivities when targeting signals in a noisy environment [39,40]. In what follows, we demonstrate analytically and numerically enhanced resolution of frequencies at the high-energy end of the spectrum of a tunable transmon device.

Resolution gain. We now turn to analyze the spectral resolution properties of *parametric spectroscopy*, benchmarked by the minimal distance that two spectral peaks must have in order to be distinguished. We illustrate the analytical calculation for the case of frequency estimation, which is equivalent to estimating the distance between the peaks if the target is the average frequency [41]. Thus, we aim to determine the central frequency ω_c of a single peaked Gaussian spectral line through relaxometry with a parametric spectroscopy sequence on a tunable transmon. The decay rate measured due to the additive signal, $\Gamma \equiv b_0^2\varphi_{ac}^2 S_{dc}(\omega_m)$, is directly related to the noise spectrum through Eq. (3), which includes the target spectral line and the background pink noise. Then, any frequency estimation is limited by σ_Γ, the uncertainty in the estimation of Γ.

The experimental procedure consists of a series of binary measurements on the transmon, where the probability of observing the qubit in its $|0\rangle$ state depends on the decoherence function and reads $p(\Gamma, t) = e^{-\Gamma t-(\alpha t)^2}$, with $\alpha = b_0\varphi_{ac}A_{ac}\sqrt{\ln(e\omega_{uv}/\omega_{ir})}$ due to the multiplicative noise source. To quantify the experimental precision in estimating Γ, we use the root mean squared error σ_Γ, which, according to the Cramér-Rao bound, is lower bound by the inverse of the Fisher information for said parameter [43,44]. Considering measurements of optimal duration T_ϕ, and assuming that the multiplicative, AC decay rate α is known and constant for different modulation frequencies, as predicted by the theoretical analysis in Eq. (3), we get that

$$I(\Gamma) = \left\langle \left(\frac{\partial \ln \mathcal{L}}{\partial \Gamma}\right)^2 \right\rangle = \frac{T_\phi^2}{e^{\Gamma T_\phi + (\alpha T_\phi)^2} - 1}, \tag{5}$$

with $\mathcal{L}$ the likelihood function for the probabilistic model for Γ. To calculate the precision in estimating Γ, we consider an experiment of total duration T_{meas}, consisting of N measurements each of duration T_ϕ and with a (small) overhead time t_m for probe initialization and readout [45]. Then, using the additivity of the Fisher information, we get that

$$\sigma_\Gamma = \sqrt{\frac{T_\phi + t_m}{T_{\text{meas}}}}\sqrt{\frac{1}{I(\Gamma)}} \approx \sqrt{\frac{1}{T_{\text{meas}}T_\phi}}. \tag{6}$$

The goal is to estimate ω_c. Assuming enough independent identical repetitions, the decay rate estimator is normally distributed. Then, the likelihood that a given decay rate x was measured for a given spectral feature with a peak frequency ω_c is equal to

$$\mathcal{L} = \frac{1}{\sigma_\Gamma\sqrt{2\pi}} \exp\left[-\frac{1}{2\sigma_\Gamma^2}\left(x - \frac{A_\omega}{\sigma_\omega\sqrt{2\pi}} e^{-\frac{(\omega-\omega_c)^2}{2\sigma_\omega^2}}\right)^2\right], \tag{7}$$

where ω is the sampled frequency and $\sigma_\omega \sim T_\phi^{-1}$ [46]. In addition, A_ω is the amplitude of the fluctuations of the energy gap due to the additive noise at the spectral peak. Then, the uncertainty of the frequency estimation is $\Delta(\omega_c) \geqslant 1/\sqrt{I(\omega_c)}$, with

$$I(\omega_c) = \left\langle \left(\frac{\partial \ln \mathcal{L}}{\partial \omega_c}\right)^2 \right\rangle = \frac{A_\omega^2 e^{-\frac{(\delta\omega)^2}{\sigma_\omega^2}}}{2\pi\sigma_\Gamma^2\sigma_\omega^6}(\delta\omega)^2, \tag{8}$$

where $\delta\omega \equiv \omega - \omega_c$. Choosing the appropriate detuning $\delta_\omega = \sigma_\omega$ that maximizes the Fisher information about the frequency, and repeating the procedure for N_ω sequences each of T_{meas} duration, yields a total $I^{\omega_c}_{\text{tot}} = \sum_{k=1}^{N_\omega} I_k \mid \delta\omega_k = \sigma_\omega$, such that the uncertainty of the estimation is

$$\Delta(\omega_c) \geqslant \left(\frac{2\pi\,\mathrm{e}}{A_\omega^2 N_\omega T_{\text{meas}} T_\phi^5}\right)^{\frac{1}{2}}. \tag{9}$$

The procedure for frequency resolution is formally equivalent: assuming knowledge of the mean frequency, the spectral distance $\epsilon \equiv \omega_c^{(1)} - \omega_c^{(2)}$ becomes the target frequency parameter [39,41,47]. There are two possible scenarios: When $\epsilon > T_\phi^{-1}$, the uncertainty is that from estimation, given by Eq. (9), and resolving the frequencies is, in principle, a matter of performing enough measurements. Conversely, when $\epsilon \ll T_\phi^{-1}$, choosing the optimal detuning, which in this case corresponds to a modulation frequency $\omega_m = (\omega_c^{(1)} + \omega_c^{(2)})/2$,

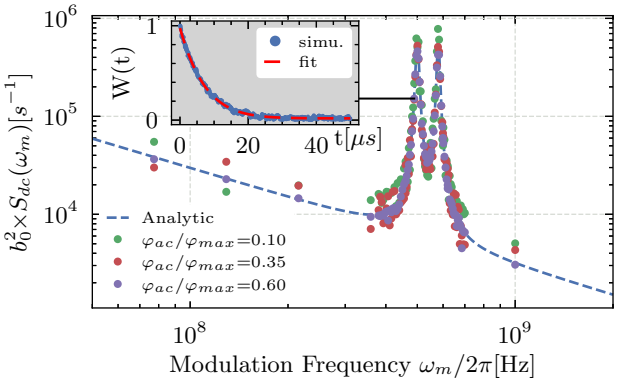


FIG. 2. Simulation of a full spectroscopy. The noise that is generated includes a pink spectrum [53] A_Φ/w with amplitude $A_\Phi \approx (60\mu\Phi_0)^2$ and two shifted AR1 processes with coherence time $T_{AR1} = 25$ ns and standard deviation $\sigma_{\Phi_e} \approx (247\mu\Phi_0)$. The centers of the AR1 spectra are located at 500 and 580 MHz, matching a distance of twice the full width at half maximum (FWHM) between the peaks. The decoherence function is estimated by averaging 2^{11} trials of numerical integration of the accumulated phase with the modulation signal, an ideal *XY*8 sequence, and the described noise. Finally, the decay rate for the specific parameters is extracted using a Gaussian and exponential fit (e.g., in the inset for $\varphi_{ac} = 0.6\varphi_{\max}$; $\omega_m/2\pi \approx$ 489 MHz) and scaled to the flux noise density using Eq. (3). We scanned 86 modulation frequencies in the 10^7–10^9 Hz range and three modulation amplitudes. The sampled points are compared to the analytical result (dashed line), showing excellent spectrum reconstruction.

yields a resolution uncertainty that approaches

$$\Delta(\epsilon) \geqslant \left(\frac{2\pi}{A_\omega^2 N_\omega T_{\text{meas}} T_\phi^7 \epsilon^2}\right)^{\frac{1}{2}} = \frac{\Delta(\omega_c)}{T_\phi \epsilon} \frac{1}{\sqrt{e}}, \qquad (10)$$

showing that resolution is limited by the finite coherence time of the probe. The advantage of parametric spectroscopy comes from its ability to achieve long coherence times for high frequencies. Therefore, uncertainties as small as 100 kHz even for GHz frequencies are within reach. Further improvement of the resolution limit imposed by Eq. (10) should be possible by considering sequential measurement schemes such as Qdyne [40,54,55], which optimize spectral resolution in noisy environments and dispel the problem of the limited coherence time of the probe [41,56]. A parametric Qdyne experiment targeting the mean frequency between two peaks would yield a signal oscillating at an ϵ frequency. Then, a sequence of evenly time-separated measurements reflects an oscillation at the peak separation frequency. For spectral features whose coherence time is longer than T_ϕ, the single-frequency limit is thus recovered, such that $\Delta(\epsilon) \gtrsim (A_\omega^2 T_\phi^4 T_{\text{meas}}^2)^{-1/2}$.

Figure 2 shows a numerical analysis of frequency resolution, in the high-frequency region of the spectrum, with parametric spectroscopy. We evaluate $W(t)$ from Eq. (3) for various modulation frequencies ω_m and amplitudes φ_{ac}, including an *XY*8 DD sequence, and both additive and multiplicative noise sources modeled as a pink noise spectrum of amplitudes $A_\Phi^{dc} \approx (35\mu\Phi_0)^2/\omega$ and A_Φ^{ac} matching $\sqrt{\langle\delta\varphi_{ac}^2\rangle}/\varphi_{ac} = 0.004\%$. Additionally, we include two Gaussian peaks with central frequencies $\omega_c^{(1)} = 500$ MHz and $\omega_c^{(2)} = 580$ MHz, both with a full width at half maximum (FWHM) of 40 MHz. Spectral reconstruction is performed by averaging, for each sampling point, 2^{11} realizations of the accumulated phase at the end of the sequence, and then fitting that average to a Gaussian and exponential decay form. The exponential decay rate estimator quantifies the additive source dephasing rate, showing excellent agreement with the analytical prediction (see SM [39]). Further, we demonstrate resolution of the central frequencies of the Gaussian features by fitting the reconstructed spectrum around the peaks to the analytical model, leaving the central frequencies, widths, and amplitudes as free fitting parameters. The resolution procedure for $\{\omega_c^{(1)}, \omega_c^{(2)}\}$ involves taking the average of 100 fits with a minimum required $R^2 > 0.8$, yielding $\omega_c^{(1)}/2\pi =$ 500 MHz, $\omega_c^{(2)}/2\pi = 570$ MHz, both with confidence bounds of $\Delta(\omega_c^{(i)})/2\pi \approx 14$ MHz, well below the FWHM of the peaks. Note that applying more stringent conditions to the fitting would permit approaching the fundamental limit imposed by the Fisher information.

The results displayed in Fig. 2 assume an infinite T_1 relaxation time. However, for high frequencies, it might be the case that $2T_1 < T_\phi$. Then, T_1 becomes the limiting factor for resolution, replacing T_ϕ in Eq. (10). In general, postselection can be applied to mitigate the effect of a short T_1 by choosing to measure dephasing only for those sample measurements that did not relax. This, however, requires a special erasure qubit construction [57,58]. The price to pay is an increase in the experiment time T_{meas} necessary to achieve the same resolution, often prohibitively so. In practice, for large $2T_1 \gg T_\phi$, postselection is not necessary, as relaxation is minimal (see Fig. 8 in the SM [39]) and results are equivalent to those with infinite T_1 in Fig. 2. On the other end, a very short $2T_1 \ll T_\phi$ causes severe degradation of the ability to estimate the peaks. Note that relaxation and dephasing are, in principle, unrelated processes, for which reason, even if for a short T_1 resolution is severely compromised, parametric spectroscopy still offers prolonged T_ϕ time.

Leakage mitigation. The two-level system approximation for superconducting qubits is limited by the unavoidable presence of higher-energy levels. Finite time drives inevitably address these unwanted levels, causing population leakage from the computational (sensing) manifold and decreasing the fidelity of operations. Leakage represents a major drawback for microwave-based operations on transmons, where it limits the gate speed imposing a minimum width for the pulses and prevents the qubit sensor from being able to accurately probe the high-energy end of the spectrum. Here, we theoretically and numerically analyze leakage during parametric spectroscopy. Our starting point is the full cosine Hamiltonian of a tunable transmon [17,38],

$$\tilde{H} = 4E_c n^2 - E_{J_{\text{eff}}}(\varphi_e)\cos(\varphi) - \dot{\varphi}_0(\varphi_e)n, \qquad (11)$$

with $E_{J,\text{eff}}(\varphi_e) = (E_{J1} + E_{J2})\sqrt{\cos^2(\varphi_e) + d^2\sin^2(\varphi_e)}$ being the effective, tunable Josephson energy, and n the charge operator. In the presence of a fast flux drive, the last term in Eq. (11) is non-negligible and causes transitions to higher levels. Around the operational point $\varphi = 0$, the phase operator φ resembles that of a bosonic field, and the full cosine

Hamiltonian (11) can be approximated by an anharmonic oscillator. The resulting Hamiltonian, including the dynamic flux drive, reads

$$H = \omega_T[\varphi_e(t)]a^\dagger a - \frac{\eta}{2}a^{\dagger 2}a^2 - \frac{\dot{\varphi}_0[\varphi_e(t)]i}{2\sqrt{\xi}}(a^\dagger - a), \quad (12)$$

with $a^\dagger(a)$ the creation (annihilation) operator, $\xi \simeq \sqrt{2E_c/(E_{J1}+E_{J2})}$, and $\varphi_0 = \tan[d\tan^{-1}(\varphi_e)] \simeq d\varphi_e$ under the quadratic approximation. $\eta > 0$ in Eq. (12) represents the anharmonicity of the transmon.

Transition to higher-energy levels is apparent in a frame rotating with the dynamic part of the qubit frequency, $\omega_T[\varphi_e(t)] - \bar{\omega}_T$, where $\bar{\omega}_T = \frac{1}{T}\int_0^T \omega_T(t)dt$ is the average energy gap during a period $T = (2\pi)/\omega_m$. The Hamiltonian in this frame, during a period of flux modulation as described in Eq. (1), reads

$$H_I = \bar{\omega}_T a^\dagger a - \frac{\eta}{2}a^{\dagger 2}a^2 - \frac{id\varphi_{ac}\omega_m}{2\sqrt{\xi}} \times \sum_{n=-\infty}^{\infty} J_n\left(\frac{\tilde{\omega}_T}{2\omega_m}\right)[e^{i(2n+1)\omega_m t}a^\dagger - e^{-i(2n+1)\omega_m t}a], \quad (13)$$

where J_n is the first Bessel function of order n and $\tilde{\omega}_T = b_0\varphi_{ac}^2/2$ is the oscillation amplitude in the qubit frequency. The Hamiltonian in Eq. (13) describes an anharmonic oscillator of frequency $\bar{\omega}_T$ perturbed by harmonic interactions with magnitudes of the Bessel series. For relevant sequence parameters, the resonance is determined by $n_{res} = \{[(\bar{\omega}_T - \eta)/\omega_m - 1]/2\} > \tilde{\omega}_T/(2\omega_m)$. Then, transitions are strongly suppressed by the properties of the Bessel function $J_n(z) \underset{n\gg z}{\sim} (z/2)^n/n!$ for positive n. Furthermore, the contribution from dispersive interaction from low-n terms can be bounded; specifically, the Rabi-like amplitude for the $|1\rangle \to |2\rangle$ transition is lower than $g^2/(g^2+\delta^2)$ with detuning and coupling,

$$\delta \equiv \bar{\omega}_T - \eta - \omega_m, \qquad g = d\omega_m\varphi_{ac}\sqrt{2/\xi}. \quad (14)$$

Figure 3 numerically analyzes the leakage for parametric spectroscopy with an *XY*8 sequence on a transmon, simulated by a diagonalized full cosine Hamiltonian projected onto the 10 lowest eigenstates. Significantly lower leakage rates with respect to spin locking, here representing a generic microwave drive procedure, are observed. This is particularly noteworthy at high frequencies, where other methods display a close to one probability of finding the population at higher levels and where, even for large modulation amplitude, parametric spectroscopy leakage rates are less than 1% of those from conventional protocols. The analytical result without pulses in Eq. (13) with Eq. (14) parameters describes well the full sequence leakage results when we apply DD sequence leakage mitigation through derivative removal by adiabatic gate [59,60], together with pulse shape optimization through maximization of the average fidelity of quantum operations [61]. Note that the slight bump appearing around 100 MHz originates on a resonance due to the DD pulses and can be addressed via a more thorough pulse optimization, tailored to the specific system that is considered. The slight *plateau* present at low frequencies is a numerical artifact of the full cosine simulation, i.e., the temporal propagation of a dynamical flux procedure with fixed flux numerically

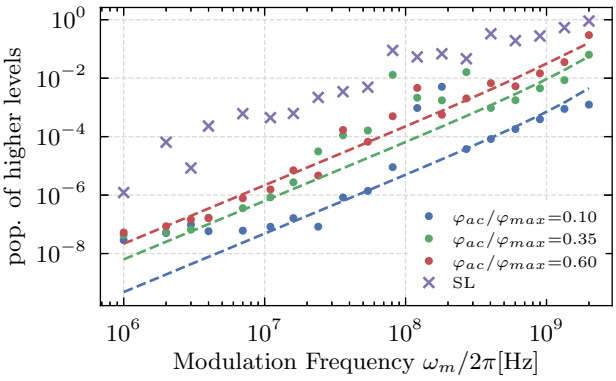


FIG. 3. Parametric spectroscopy leakage analysis. Results of simulated (dots) 10 μs modulation and *XY*8 pulse sequence, applied to the full cosine tunable transmon Hamiltonian (11), with $\omega_{\max}/2\pi = 6$ GHz, $\eta/2\pi = 300$ MHz, and $d \approx 1/3$. Each dot represents the average maximal population outside the $\{|0\rangle, |1\rangle\}$ (computational or sensing) subspace during the last 10 time steps (0.1 ns) of the simulated dynamics (see SM [39]), thus mitigating phase variability of the many active multilevel interactions. The dashed lines correspond to the analytical result for parametric modulation without DD from Eq. (13) with the parameters from Eq. (14). The violet × marks represent the numerical results for an analog spin-locking Hamiltonian (the horizontal axis being the Rabi frequency Ω). Simulations were performed using QUTIP [62].

diagonalized n, φ operators introduces additional leakage that is not expected to be observed in an experiment. These results justify the two-level approximation employed to demonstrate high resolution with parametric spectroscopy.

Discussion. Full spectral reconstruction of the noise interacting with a quantum system is critical for the development of quantum technologies. Here we demonstrate how tunable transmons serve as precise quantum sensors of the high-frequency noise spectrum. Combining parametric modulation with dynamical decoupling allows the creation of custom narrow frequency filters capable of extending the frequency range of the tunable transmon spectrometer into the GHz region, with unrivaled frequency resolution. We show great adaptability across the spectrum, increased coherence survival, and a significant reduction in leakage to higher-energy levels.

Any sensing protocol requires a trade-off between the amplitude of the control pulses, the target frequency, the desired resolution, and leakage minimization. Unlike alternative strategies that require large modulation amplitudes that shorten coherence time and degrade attainable resolution [35–37,63], parametric spectroscopy has the unique advantage of allowing greater flexibility with innately built noise resilience when operated at close vicinity to a sweet spot. Moreover, it benefits from noise mitigation strategies that can be directly applied to the DD sequence, permitting larger amplitudes with reduced leakage and, thereby, increasing the sensitivity at high frequencies without compromising the spectrometer. Further, the protocol that we describe can be used to address structures in the spectrum reflected through noise correlations [39,64], and can be generalized to any system holding tunable energy gaps and therefore has the

potential to become a useful addition to the quantum sensing toolbox.

Acknowledgments. The contents of this Letter have greatly benefited from fruitful discussions with Ido Zuk and Yotam Vaknin. S.O.-C. acknowledges support from the María Zambrano Fellowship. A.R. acknowledges the support of ERC grant QRES, Project No. 770929, Quantera grant MfQDS, the Israeli Science foundation (ISF), the Schwartzmann university chair and the Israeli Innovation Authority under the project Quantum Computing Infrastructures.

[1] J. Preskill, Quantum computing in the NISQ era and beyond, Quantum **2**, 79 (2018).
[2] E. L. Hahn, Spin echoes, Phys. Rev. **80**, 580 (1950).
[3] H. Y. Carr and E. M. Purcell, Effects of diffusion on free precession in nuclear magnetic resonance experiments, Phys. Rev. **94**, 630 (1954).
[4] S. Meiboom and D. Gill, Modified spin-echo method for measuring nuclear relaxation times, Rev. Sci. Instrum. **29**, 688 (1958).
[5] L. Viola and S. Lloyd, Dynamical suppression of decoherence in two-state quantum systems, Phys. Rev. A **58**, 2733 (1998).
[6] L. Viola, E. Knill, and S. Lloyd, Dynamical decoupling of open quantum systems, Phys. Rev. Lett. **82**, 2417 (1999).
[7] Ł. Cywiński, R. M. Lutchyn, C. P. Nave, and S. Das Sarma, How to enhance dephasing time in superconducting qubits, Phys. Rev. B **77**, 174509 (2008).
[8] A. M. Souza, G. A. Álvarez, and D. Suter, Robust dynamical decoupling for quantum computing and quantum memory, Phys. Rev. Lett. **106**, 240501 (2011).
[9] D. Suter and G. A. Álvarez, *Colloquium:* Protecting quantum information against environmental noise, Rev. Mod. Phys. **88**, 041001 (2016).
[10] A. G. Kofman and G. Kurizki, Universal dynamical control of quantum mechanical decay: Modulation of the coupling to the continuum, Phys. Rev. Lett. **87**, 270405 (2001).
[11] A. G. Kofman and G. Kurizki, Unified theory of dynamically suppressed qubit decoherence in thermal baths, Phys. Rev. Lett. **93**, 130406 (2004).
[12] M. J. Biercuk, A. C. Doherty, and H. Uys, Dynamical decoupling sequence construction as a filter-design problem, J. Phys. B: At. Mol. Opt. Phys. **44**, 154002 (2011).
[13] G. A. Álvarez and D. Suter, Measuring the spectrum of colored noise by dynamical decoupling, Phys. Rev. Lett. **107**, 230501 (2011).
[14] J. Bylander, S. Gustavsson, F. Yan, F. Yoshihara, K. Harrabi, G. Fitch, D. G. Cory, Y. Nakamura, J.-S. Tsai, and W. D. Oliver, Noise spectroscopy through dynamical decoupling with a superconducting flux qubit, Nat. Phys. **7**, 565 (2011).
[15] T. Yuge, S. Sasaki, and Y. Hirayama, Measurement of the noise spectrum using a multiple-pulse sequence, Phys. Rev. Lett. **107**, 170504 (2011).
[16] K. C. Young and K. B. Whaley, Qubits as spectrometers of dephasing noise, Phys. Rev. A **86**, 012314 (2012).
[17] P. Krantz, M. Kjaergaard, F. Yan, T. P. Orlando, S. Gustavsson, and W. D. Oliver, A quantum engineer's guide to superconducting qubits, Appl. Phys. Rev. **6**, 021318 (2019).
[18] F. Yan, S. Gustavsson, J. Bylander, X. Jin, F. Yoshihara, D. G. Cory, Y. Nakamura, T. P. Orlando, and W. D. Oliver, Rotating-frame relaxation as a noise spectrum analyser of a superconducting qubit undergoing driven evolution, Nat. Commun. **4**, 2337 (2013).
[19] G. Ithier, E. Collin, P. Joyez, P. J. Meeson, D. Vion, D. Esteve, F. Chiarello, A. Shnirman, Y. Makhlin, J. Schriefl, and G. Schön, Decoherence in a superconducting quantum bit circuit, Phys. Rev. B **72**, 134519 (2005).
[20] D. Sank, R. Barends, R. C. Bialczak, Y. Chen, J. Kelly, M. Lenander, E. Lucero, M. Mariantoni, A. Megrant, M. Neeley, P. J. J. O'Malley, A. Vainsencher, H. Wang, J. Wenner, T. C. White, T. Yamamoto, Y. Yin, A. N. Cleland, and J. M. Martinis, Flux noise probed with real time qubit tomography in a Josephson phase qubit, Phys. Rev. Lett. **109**, 067001 (2012).
[21] F. Yan, J. Bylander, S. Gustavsson, F. Yoshihara, K. Harrabi, D. G. Cory, T. P. Orlando, Y. Nakamura, J.-S. Tsai, and W. D. Oliver, Spectroscopy of low-frequency noise and its temperature dependence in a superconducting qubit, Phys. Rev. B **85**, 174521 (2012).
[22] O. Astafiev, Y. A. Pashkin, Y. Nakamura, T. Yamamoto, and J. S. Tsai, Quantum noise in the Josephson charge qubit, Phys. Rev. Lett. **93**, 267007 (2004).
[23] F. Yoshihara, Y. Nakamura, F. Yan, S. Gustavsson, J. Bylander, W. D. Oliver, and J.-S. Tsai, Flux qubit noise spectroscopy using Rabi oscillations under strong driving conditions, Phys. Rev. B **89**, 020503(R) (2014).
[24] F. Yan, S. Gustavsson, A. Kamal, J. Birenbaum, A. P. Sears, D. Hover, T. J. Gudmundsen, D. Rosenberg, G. Samach, S. Weber, J. L. Yoder, T. P. Orlando, J. Clarke, A. J. Kerman, and W. D. Oliver, The flux qubit revisited to enhance coherence and reproducibility, Nat. Commun. **7**, 12964 (2016).
[25] E. Paladino, Y. M. Galperin, G. Falci, and B. L. Altshuler, 1/*f* noise: Implications for solid-state quantum information, Rev. Mod. Phys. **86**, 361 (2014).
[26] P. Bertet, C. J. P. M. Harmans, and J. E. Mooij, Parametric coupling for superconducting qubits, Phys. Rev. B **73**, 064512 (2006).
[27] S. A. Caldwell, N. Didier, C. A. Ryan, E. A. Sete, A. Hudson, P. Karalekas, R. Manenti, M. P. da Silva, R. Sinclair, E. Acala, N. Alidoust, J. Angeles, A. Bestwick, M. Block, B. Bloom, A. Bradley, C. Bui, L. Capelluto, R. Chilcott, J. Cordova *et al.*, Parametrically activated entangling gates using transmon qubits, Phys. Rev. Appl. **10**, 034050 (2018).
[28] A. O. Niskanen, Y. Nakamura, and J.-S. Tsai, Tunable coupling scheme for flux qubits at the optimal point, Phys. Rev. B **73**, 094506 (2006).
[29] A. O. Niskanen, K. Harrabi, F. Yoshihara, Y. Nakamura, S. Lloyd, and J. S. Tsai, Quantum coherent tunable coupling of superconducting qubits, Science **316**, 723 (2007).
[30] F. Beaudoin, M. P. da Silva, Z. Dutton, and A. Blais, First-order sidebands in circuit QED using qubit frequency modulation, Phys. Rev. A **86**, 022305 (2012).
[31] B. Royer, A. L. Grimsmo, N. Didier, and A. Blais, Fast and high-fidelity entangling gate through parametrically modulated longitudinal coupling, Quantum **1**, 11 (2017).

[32] T. Roy, S. Kundu, M. Chand, S. Hazra, N. Nehra, R. Cosmic, A. Ranadive, M. P. Patankar, K. Damle, and R. Vijay, Implementation of pairwise longitudinal coupling in a three-qubit superconducting circuit, Phys. Rev. Appl. **7**, 054025 (2017).

[33] D. C. McKay, S. Filipp, A. Mezzacapo, E. Magesan, J. M. Chow, and J. M. Gambetta, Universal gate for fixed-frequency qubits via a tunable bus, Phys. Rev. Appl. **6**, 064007 (2016).

[34] M. Reagor, C. B. Osborn, N. Tezak, A. Staley, G. Prawiroatmodjo, M. Scheer, N. Alidoust, E. A. Sete, N. Didier, M. P. da Silva, E. Acala, J. Angeles, A. Bestwick, M. Block, B. Bloom, A. Bradley, C. Bui, S. Caldwell, L. Capelluto, R. Chilcott *et al.*, Demonstration of universal parametric entangling gates on a multi-qubit lattice, Sci. Adv. **4**, eaao3603 (2018).

[35] S. S. Hong, A. T. Papageorge, P. Sivarajah, G. Crossman, N. Didier, A. M. Polloreno, E. A. Sete, S. W. Turkowski, M. P. da Silva, and B. R. Johnson, Demonstration of a parametrically activated entangling gate protected from flux noise, Phys. Rev. A **101**, 012302 (2020).

[36] N. Didier, E. A. Sete, J. Combes, and M. P. da Silva, AC flux sweet spots in parametrically modulated superconducting qubits, Phys. Rev. Appl. **12**, 054015 (2019).

[37] J. A. Valery, S. Chowdhury, G. Jones, and N. Didier, Dynamical sweet spot engineering via two-tone flux modulation of superconducting qubits, PRX Quantum **3**, 020337 (2022).

[38] J. Koch, T. M. Yu, J. Gambetta, A. A. Houck, D. I. Schuster, J. Majer, A. Blais, M. H. Devoret, S. M. Girvin, and R. J. Schoelkopf, Charge-insensitive qubit design derived from the Cooper pair box, Phys. Rev. A **76**, 042319 (2007).

[39] See Supplemental Material at http://link.aps.org/supplemental/10.1103/PhysRevResearch.7.L012056 for a detailed derivation of the decoherence function for parametric spectroscopy, a sensitivity analysis of parametric modulation and comparison to spin locking, a signal-to-noise ratio analysis of the method, a complete derivation of the resolution limits, details on the leakage analysis through the full cosine model, additional details on the numerical simulations and the derivation of the Fisher information equations, details of the leakage analysis, a brief discussion about the possibility of measuring correlations in the environment with parametric spectroscopy, and an analysis of the effect of T_1, which also includes Refs. [40,42–45,48–52,61,62].

[40] J. M. Boss, K. S. Cujia, J. Zopes, and C. L. Degen, Quantum sensing with arbitrary frequency resolution, Science **356**, 837 (2017).

[41] T. Gefen, A. Rotem, and A. Retzker, Overcoming resolution limits with quantum sensing, Nat. Commun. **10**, 4992 (2019).

[42] S. Oviedo-Casado, A. Rotem, R. Nigmatullin, J. Prior, and A. Retzker, Correlated noise in Brownian motion allows for super resolution, Sci. Rep. **10**, 19691 (2020).

[43] H. Cramér, *Mathematical Methods of Statistics (PMS-9),* (Princeton University Press, Princeton, 1946), Vol. 9.

[44] C. R. Rao, Information and the accuracy attainable in the estimation of statistical parameters, in *Breakthroughs in Statistics: Foundations and Basic Theory*, edited by S. Kotz and N. L. Johnson (Springer, New York, 1992), pp. 235–247.

[45] C. L. Degen, F. Reinhard, and P. Cappellaro, Quantum sensing, Rev. Mod. Phys. **89**, 035002 (2017).

[46] J. F. Barry, J. M. Schloss, E. Bauch, M. J. Turner, C. A. Hart, L. M. Pham, and R. L. Walsworth, Sensitivity optimization for NV-diamond magnetometry, Rev. Mod. Phys. **92**, 015004 (2020).

[47] A. Rotem, T. Gefen, S. Oviedo-Casado, J. Prior, S. Schmitt, Y. Burak, L. McGuiness, F. Jelezko, and A. Retzker, Limits on spectral resolution measurements by quantum probes, Phys. Rev. Lett. **122**, 060503 (2019).

[48] T. Walter, P. Kurpiers, S. Gasparinetti, P. Magnard, A. Potočnik, Y. Salathé, M. Pechal, M. Mondal, M. Oppliger, C. Eichler, and A. Wallraff, Rapid high-fidelity single-shot dispersive readout of superconducting qubits, Phys. Rev. Appl. **7**, 054020 (2017).

[49] J. Tuorila, M. Partanen, T. Ala-Nissila, and M. Möttönen, Efficient protocol for qubit initialization with a tunable environment, npj Quantum Inf. **3**, 27 (2017).

[50] Y. Sunada, S. Kono, J. Ilves, S. Tamate, T. Sugiyama, Y. Tabuchi, and Y. Nakamura, Fast readout and reset of a superconducting qubit coupled to a resonator with an intrinsic Purcell filter, Phys. Rev. Appl. **17**, 044016 (2022).

[51] L. Rayleigh F. R. S., Investigations in optics, with special reference to the spectroscope, Lond. Edinb. Dubl. Phil. Mag. J. Sci. **8**, 261 (1879).

[52] G. E. P. Box, G. M. Jenkins, and G. C. Reinsel, *Time Series Analysis: Forecasting and Control*, 3rd ed. (Prentice Hall, Englewood Cliffs, NJ, 1994), Chap. 3.2.

[53] J. Timmer and M. Koenig, On generating power law noise, Astron. Astrophys. **300**, 707 (1995).

[54] S. Schmitt, T. Gefen, F. M. Stürner, T. Unden, G. Wolff, C. Müller, J. Scheuer, B. Naydenov, M. Markham, S. Pezzagna, J. Meijer, I. Schwarz, M. Plenio, A. Retzker, L. P. McGuinness, and F. Jelezko, Submillihertz magnetic spectroscopy performed with a nanoscale quantum sensor, Science **356**, 832 (2017).

[55] D. R. Glenn, D. B. Bucher, J. Lee, M. D. Lukin, H. Park, and R. L. Walsworth, High-resolution magnetic resonance spectroscopy using a solid-state spin sensor, Nature (London) **555**, 351 (2018).

[56] N. Staudenmaier, A. Vijayakumar-Sreeja, G. Genov, D. Cohen, C. Findler, J. Lang, A. Retzker, F. Jelezko, and S. Oviedo-Casado, Optimal sensing protocol for statistically polarized nano-NMR with NV centers, Phys. Rev. Lett. **131**, 150801 (2023).

[57] A. Kubica, A. Haim, Y. Vaknin, H. Levine, F. Brandão, and A. Retzker, Erasure qubits: Overcoming the T_1 limit in superconducting circuits, Phys. Rev. X **13**, 041022 (2023).

[58] H. Levine, A. Haim, J.S.C. Hung, N. Alidoust, M. Kalaee, L. DeLorenzo, E.A. Wollack, P. Arrangoiz-Arriola, A. Khalajhedayati, R. Sanil, H. Moradinejad, Y. Vaknin, A. Kubica, D. Hover, S. Aghaeimeibodi, J.A. Alcid, C. Baek, J. Barnett, K. Bawdekar, P. Bienias *et al.*, Demonstrating a long-coherence dual-rail erasure qubit using tunable transmons, Phys. Rev. X **14**, 011051 (2024).

[59] F. Motzoi, J. M. Gambetta, P. Rebentrost, and F. K. Wilhelm, Simple pulses for elimination of leakage in weakly nonlinear qubits, Phys. Rev. Lett. **103**, 110501 (2009).

[60] J. M. Gambetta, F. Motzoi, S. T. Merkel, and F. K. Wilhelm, Analytic control methods for high-fidelity unitary operations in a weakly nonlinear oscillator, Phys. Rev. A **83**, 012308 (2011).

[61] M. A. Nielsen, A simple formula for the average gate fidelity of a quantum dynamical operation, Phys. Lett. A **303**, 249 (2002).

[62] J. Johansson, P. Nation, and F. Nori, QuTiP: An open-source Python framework for the dynamics of open quantum systems, Comput. Phys. Commun. **183**, 1760 (2012).

[63] Z. Huang, P. S. Mundada, A. Gyenis, D. I. Schuster, A. A. Houck, and J. Koch, Engineering dynamical sweet spots to protect qubits from $1/f$ noise, Phys. Rev. Appl. **15**, 034065 (2021).

[64] U. von Lüpke, F. Beaudoin, L. M. Norris, Y. Sung, R. Winik, J. Y. Qiu, M. Kjaergaard, D. Kim, J. Yoder, S. Gustavsson, L. Viola, and W. D. Oliver, Two-qubit spectroscopy of spatiotemporally correlated quantum noise in superconducting qubits, PRX Quantum **1**, 010305 (2020).